

Short Communication

A New Triphosphate $\text{TlFeHP}_3\text{O}_{10}$: Synthesis, Crystal Structure, Tl^+ and Proton Conduction Pathways

Eya Rezgui¹, Riadh Marzouki^{2,1,3*}, Mutasem Z. Bani-Fwaz², and Najoua Ouerfelli¹

¹ Laboratory of Materials, Crystallochemistry and Applied Thermodynamics, Faculty of Sciences of Tunis, University of Tunis El Manar, Tunisia.

² Chemistry Department, College of Science, King Khalid University, Abha 61413, Saudi Arabia.

³ Chemistry Department, Faculty of Sciences of Sfax, University of Sfax, 3038, Tunisia.

*E-mail: riadh.marzouki@hotmail.fr, rmarzouki@kku.edu.sa

Received: 5 May 2020/ Accepted: 5 July 2020 / Published: 10 August 2020

A new triphosphate $\text{TlFeHP}_3\text{O}_{10}$ was obtained by the hydrothermal method. It crystallizes in the monoclinic space group $C2/c$ with $a=11.994$ (5), $b= 8.476$ (2), $c=9.276$ (3), $\beta=111.99$ (3), $V=874.4$ (5) and $Z=4$. The structure was determined by single-crystal X-ray diffraction data collection and provides a clear identification of hydrogen bonds interconnecting the triphosphoric groups in order to build HP_3O_{10} connected by FeO_6 octahedra sharing corners. Thallium cations are located in tunnels. This arrangement was confirmed by CHARDI and BVS models. IR spectrum confirms that most of the vibrational modes are comparable to similar triphosphates and to the calculated frequencies. BVSP and BVSE models were used to simulate conduction pathways migration in the three dimensional framework. The Bond valence analysis revealed that Tl^+ conductivity was one dimensional insured by crystal sites with an activation energy 0.664 eV. However, H^+ conductivity was insured by both crystal sites and interstitials with 0.682 eV migration energy for one dimensional conductivity and 1.293 eV for three dimensional migrations.

Keywords: Triphosphate, Crystal structure, Ionic conductivity, Bond valence analysis, Vibrational study.

1. INTRODUCTION

The triphosphates were studied with mineral cations like $\text{NaZn}_2\text{P}_3\text{O}_{10} \cdot 9\text{H}_2\text{O}$ [1], $\text{Sr}_3\text{P}_3\text{O}_{10}\text{Cl}$ [2] and $\text{CsAl}_2\text{BP}_6\text{O}_{20}$ [3]. Several mineral compounds with acidic triphosphoric anions have been reported, for example, $\text{CsVHP}_3\text{O}_{10}$ [4], $(\text{NH}_4)\text{CrHP}_3\text{O}_{10}$ [5], $(\text{H}_3\text{O})\text{FeHP}_3\text{O}_{10}$ [6], $(\text{NH}_4)\text{VHP}_3\text{O}_{10}$ [7], $(\text{NH}_4)\text{AlHP}_3\text{O}_{10}$ [8] and $\text{KAlHP}_3\text{O}_{10}$ [8]. The inorganic triphosphates in particular $\text{AMnHP}_3\text{O}_{10}$ where A is a monovalent cation has been widely studied due to their ferromagnetic and electric properties [9, 10]. They are well known for their open frame works such as $\text{KSmHP}_3\text{O}_{10}$ [11], $\text{NH}_4\text{SmHP}_3\text{O}_{10}$ [11],

$\text{NH}_4\text{BiHP}_3\text{O}_{10}$ [12], $\text{CsGaHP}_3\text{O}_{10}$ [13] and $\text{RbPrHP}_3\text{O}_{10}$ [14] especially for significant mobility of alkalis and protons in the structure [15]. The present work describes the preparation and structural investigation of a new triphosphate $\text{TlFeHP}_3\text{O}_{10}$. We also report here the vibrational and the bond valence sum of the ionic conductivity study of the title compound.

2. EXPERIMENTAL

2.1. Synthesis and characterization

$\text{TlFeHP}_3\text{O}_{10}$ has been synthesized using the hydrothermal method by mixing 0.990g TlNO_3 , 1.113g $\text{Fe}(\text{NO}_3)_3 \cdot 9\text{H}_2\text{O}$, and 4.10 mL H_3PO_4 ($\geq 85\%$). The obtained solution was heated to 80°C and stirred with 10 ml of deionized water. The reaction preparation was then poured into a Teflon-lined stainless steel autoclave, 40% filled, and taken to 180°C temperature under autogenous pressure for 7 days. Then, the solution was gradually cooled to room temperature and washed with distilled water various times. Prism shaped light pink transparent single crystals were obtained. The single phase has been lately confirmed by X-ray diffraction (Fig. 1).

The infrared spectrum was recorded at room temperature in the frequency range $4000\text{--}400\text{ cm}^{-1}$. The spectrometer used is a Nicolet 200 FT-IR spectrophotometer powered by OMNIC Spectra software.

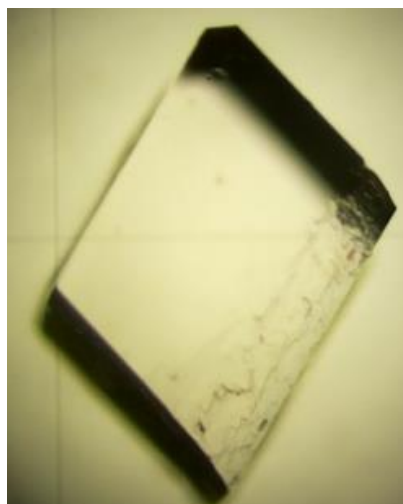


Figure 1. Polarizing microscope image of a $\text{TlFeHP}_3\text{O}_{10}$ phase crystal.

2.2. X-ray data collection and structure refinement

The X-ray diffraction intensities were collected using an Enraf-Nonius CAD-4 diffractometer equipped with a graphite monochromator of Mo K_α radiation ($\lambda = 0.71073 \text{ \AA}$) (ω - 2θ scan) [16, 17]. 2410 reflections were measured for 949 independent reflections. Since the elaborated compound is

isotype to $(\text{NH}_4)\text{FeHP}_3\text{O}_{10}$ [7] the structure has been solved in $C2/c$ space group using Patterson heavy atom method provided by the SHELX computer programs [18] included in the WingX software package [19]. The Patterson heavy atom method helped obtaining the positions of the iron and phosphorus atoms and successive Fourier analysis allowed the other atoms to be located. At this stage, an empirical absorption correction by ψ -scan [20] was applied. The rest of the atoms of the structure were located by Fourier difference. The structure was lastly refined by fixing the occupancy of Tl1 and Tl2 at 0.52(4) and 0.24(2) respectively with setting the same U_{eq} for them by using the appropriate procedures (SUMP, EADP, FVAR). The highest remaining electron density is located at 0.74 Å from Tl2. The slightly elevated residue on the thallium side is attributed to its free doublet [21].

The final refinement based on F^2 of all atoms converges to the following values of reliability factors: $R(F) = 0.067$ and $wR(F^2) = 0.163$.

The crystallographic data for $\text{TlFeHP}_3\text{O}_{10}$ is summarized in Table 1. The atomic coordinates, fractional occupancies and isotropic thermal atomic factors Table 2.

Table 1. Crystal data and structure refinement for $\text{TlFeHP}_3\text{O}_{10}$.

<i>Crystal data</i>	
Empirical formula	$\text{TlFeHP}_3\text{O}_{10}$
Crystal system; Space group	Monoclinic, $C2/c$
Unit cell dimensions	a=11.994 (5)(Å) b= 8.476 (2)(Å) c= 9.276 (3)(Å) $\beta = 111.99 (3) (^\circ)$
Formula weight; Density ρ_{cal}	514.14 g mol^{-1} ; 3.906 $\text{g}\cdot\text{cm}^{-3}$
V (Å ³), Z	874.4 (5); 4
Temperature, K	298(2)
Radiation; λ , (Å)	Mo K_{α} ; 0.71073
Crystal size (mm)	0.65 × 0.50 × 0.40
Crystal color; Shape	Pink, Prism
Absorption coefficient μ ; F(000)	19.97 mm^{-1} ; 928
<i>Data collection</i>	
Diffractometer	Enraf-Nonius CAD-4
Scan mode	$\omega/2\theta$
θ range of data collection, deg	3.0 - 27.0
Limiting indices h, k, l	-15 ≤ h ≤ 15 -2 ≤ k ≤ 10 -11 ≤ l ≤ 11
Number of reflections: measured/independent	2410 / 949 [$R_{\text{int}} = 0.081$]
Number of reflections with $I \geq 2\sigma(I)$	881
Absorption correction; $T_{\text{min}}, T_{\text{max}}$	ψ scan; 0.303/ 0.781
<i>Refinement</i>	
Refinement method	Full-matrix least-squares on F^2
Parameters/Restraints	55/1
$R(F^2)$; $wR(F^2)$	0.067; 0.163
Extinction coefficient	0.063 (4)
$\Delta\rho$ max ; $\Delta\rho$ min ($\text{e}\cdot\text{Å}^{-3}$)	4,32 ; -2,27
Goodness-of-Fit on F^2	1.05

Table 2. Atomic coordinates and equivalent displacement parameters (\AA^2) for $\text{TlFeHP}_3\text{O}_{10}$.

Atom	Wyck	x	y	z	$U_{eq}^*, \text{\AA}^2$	Occ. (<1)
Fe1	8f	0.25	0.75	0.5	0.0011 (5)*	
P1	8e	0.20942(2)	0.4339 (2)	0.2955(2)	0.0030 (5)*	
P2	4a	0.5	0.1249 (3)	0.25	0.0037 (6)*	
O1	8e	0.1768 (5)	0.2996 (8)	0.3798 (6)	0.015 (1)	
O2	8f	0.4180 (5)	0.0124 (7)	0.3048 (6)	0.009 (1)*	
O3	16g	0.2591 (5)	0.3840 (8)	0.1773 (6)	0.012 (1)	
O4	16g	0.4266 (4)	0.2187 (7)	0.1089 (5)	0.007 (1)*	
O6	16g	0.2878 (5)	0.5586 (5)	0.4032 (6)	0.007 (1)	
Tl1	8f	0	0.059 (1)	0.25	0.027 (3)	0.52 (4)
Tl2	16g	0.007 (1)	0.0644 (9)	0.219 (4)	0.027 (3)	0.24 (2)
H1	8e	0.25	0.25	0.5	0.08 (8)*	

* U_{eq} is defined as one-third of the trace of the orthogonalized U_{ij} tensor.

2.3. BVS and CHARDI validation

The proposed structured model was confirmed by both methods charge distribution CHARDI [22, 23] and bond valence sum BVS [24, 25] using CHARDI2015 [26] and SoftBV [25] programs respectively

CHARDI model shows that the effective coordination numbers (ECoNs) are 3.89 and 3.90 for P1O_4 and P2O_4 respectively which confirms that both tetrahedrons are slightly distorted (Table 3). These results are in good agreement with those usually met in triphosphate anions. FeO_6 octahedra is nearly regular. The Fe-O distance varies from 1.968(5) to 1.994(5) \AA and the ECoN is 1.983 \AA .

Table 3. CHARDI and BVS analysis of cationpolyhedra in $\text{TlFeHP}_3\text{O}_{10}$.

Cation	$q(i).\text{sof}(i)$	$Q(i)$	$V(i)$	CN(i)	ECoN(i)
Tl1	0.52	0.52	0.05	8	8.54
Tl2	0.24	0.24	0.913	8	8.00
P1	5.00	5.01	5.040	4	3.89
P2	5.00	5.02	4.938	4	3.90
Fe1	3.00	2.97	3.203	6	5.99
H1	1.00	0.99	1.012	2	2.00

Notes: $q(i)$ = formal oxidation number; $\text{sof}(i)$ = site occupation factor; CNs = coordination number ($\text{thallium CNs for } d(\text{Tl-O})_{\text{max}} = 3,40\text{\AA}$); ECoN(i) = number of effective coordination; σ = dispersion factor on cationic charges measuring the deviation of the computed charges (Q) with respect to the formal oxidation numbers; $\sigma_{\text{cat}} = [\sum i(q_i - Q_i)^2 / N - 1]^{1/2} = 0.005$.

The validity of the structural model in particular the distribution of M1 (Tl1/Tl2) site was well confirmed by CHARDI and BVS models. CHARDI method shows a cationic charge distribution factor $\sigma_{\text{cat}} = 0.5\%$ (Table 3). The BVS analysis exhibits that calculated charge values $Q(i)$ and valences $V(i)$ match well the weighted oxidation numbers by occupation rates with a factor $G_{II} = 0.094$ v.u (global

instability index) [27]. Table 4 shows that the P2O₄ tetrahedron has a slight distortion compared to the P1O₄ tetrahedron and a low distortion at the Fe-O bond level for the Fe1O₆ octahedra.

Table 4. Distortion indices (*DI*) for the coordination polyhedra around Fe and P in TlFeHP₃O₁₀.

	P1	P2	Fe1
<i>DI_d</i>	0.013	0.020	0.027
<i>DI_a</i>	0.024	0.050	0.044
<i>DI_o</i>	0.013	0.035	0.035
<i>DI_d</i> = $\sum_{i=1}^{n_1} (d_i - d_m)/n_1 d_m$; <i>DI_a</i> = $\sum_{i=1}^{n_2} (a_i - a_m)/n_2 a_m$ and <i>DI_o</i> = $\sum_{i=1}^{n_2} (o_i - o_m)/n_2 o_m$. <i>d</i> , <i>a</i> and <i>o</i> signify Fe/P-O bond distance, O-Fe/P-O angle and O-O edge within the relevant polyhedron; index <i>i</i> indicates individual values, index <i>m</i> the mean value for the polyhedron. <i>n1</i> and <i>n2</i> are 4 and 6 for the arsenate tetrahedral; 6 and 12 for the iron octahedral.			

2.4. Bond valence pathway models

Relationships between bond length *R* and bond valence *s*

$$S_{A-X} = \exp\left(\frac{R_0 - R_{A-X}}{b}\right) \quad (1)$$

are commonly used in crystal chemistry to identify plausible equilibrium sites for an atom in a structure as sites where the BV sum of the atom agrees with its oxidation state [28]. Recently a systematic adjustment of the empirical BV parameters (*b* and *R*₀ in eqn 1) was introduced to the bond softness [29]. The resulting BV parameter set, softBV, [25] and the inclusion of interactions beyond the first coordination shell, permits more adequate estimates of non-equilibrium site energies. Originally the interactions between cations *A* and anions *X* were expressed in arbitrary “valence units”. However, they may be also related, as demonstrated recently [30, 31], to an absolute energy scale by expressing the bond valence as a Morse-type potential. In this approach, the ionic transport pathway are identified as regions of low site energy *E*(*A*)

$$E(A) = D_0 \left[\sum_{i=1}^N \left(\frac{s_{A-X_i} - s_{min,A-X_i}}{s_{min,A-X_i}} \right)^2 - N \right] + E_{Coulomb}(A - B) \quad (2)$$

where the second term accounts for Coulomb interactions between mobile ions and framework:

$$E_{Coulomb}(A - B) = 14.4 \frac{eV}{\text{\AA}} \frac{z_A z_B}{R_{A-B}} \operatorname{erfc}\left(\frac{R_{A-B}}{\rho_0}\right) \quad (3)$$

The fractional ion charges *z_A*, *z_B* are derived from the nominal charges and principal quantum numbers by the formalism explained in [30, 31]

Coulomb attraction terms are generally integrated in the Morse attraction term. The activation energy required for the migration of a cation from a site *A* to a site *B* is the difference between the site energy (*B*) and the site energy (*A*):

$$E_a = E(B) - E(A).$$

The Bond Valence Sum Pathways BVSP calculations were performed using JUMPITER software [32]. The atoms used in our calculation are located in a sphere of radius 20 Å. A beam of size

0.06 Å and a pitch of 0.1 Å, with a mesh distance of 0.02 Å between the points of the belt, were used [33].

The Bond Valence Bond Valence Site Energy (BVSE) calculations were accomplished using Tl^+ and H^+ as test ions and 0.1 Å resolution grid. The BVSE isosurfaces were visualized using the VESTA 3 program [34].

3. RESULTS AND DISCUSSION

3.1. Structure description and discussion

The crystal structural of $\text{TlFeHP}_3\text{O}_{10}$ compound is isotopic to $(\text{NH}_4)\text{FeHP}_3\text{O}_{10}$ [7], and it crystallizes in the monoclinic system with space group $C2/c$. The asymmetric unit is formed of FeO_6 octahedra, two tetrahedrons of the P_3O_6 group, one of which (P_2O_4) is located on axis 2, and a statistically disordered thallium cation on two positions (Tl1 and Tl2) (Fig. 2).

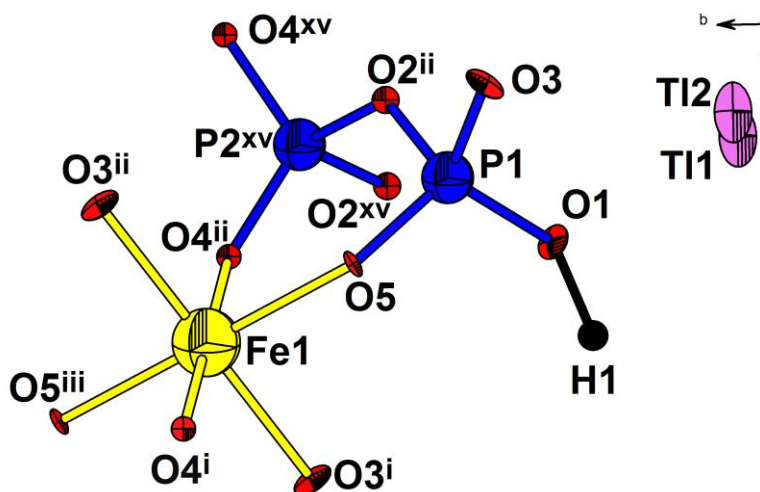


Figure 2. Asymmetric unit of $\text{TlFeHP}_3\text{O}_{10}$ compound.

The structure of $\text{TlFeHP}_3\text{O}_{10}$ compound is characterized by a Three-dimensional anionic framework $\text{FeHP}_3\text{O}_{10}$ formed by triphosphate groups HP_3O_{10} connected by FeO_6 octahedra sharing corners (Fig. 3). This arrangement leads to tunnels along c direction where thallium cations are located. According to the literature, all compounds of $\text{A}^{\text{I}}\text{M}^{\text{III}}\text{HP}_3\text{O}_{10}$ formula adopt two-dimensional anionic frameworks where the monovalent cations occupy the interlayer spaces [35-36]. However, those which crystallize in $C2$ [36-38] and $C2/c$ [4-9, 10,] space groups have three-dimensional structures with tunnels along c axis where the monovalent cations are housed.

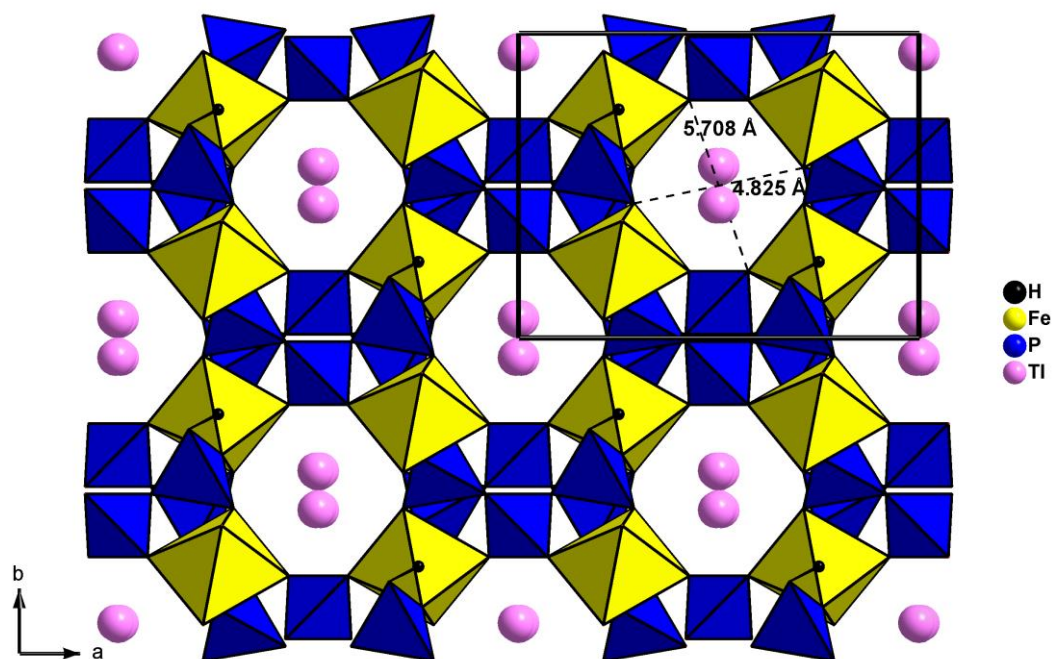


Figure 3. Projection of the $\text{TlFeHP}_3\text{O}_{10}$ structure in the $[001]$ direction.

$(\text{HP}_3\text{O}_{10})^{-4}$ groups are linked with a short $\text{O}-\text{H} \cdots \text{O}$ (1.207\AA) symmetric hydrogen bonding. The H atom is located at a centre of symmetry between two O (2) atoms (Fig. 4). Similar symmetric $\text{O} \cdots \text{H} \cdots \text{O}$ hydrogen bonding was encountered in $\text{RbMnHP}_3\text{O}_{10}$ [9], $\text{KMnHP}_3\text{O}_{10}$ [10] and $\text{CsMnHP}_3\text{O}_{10}$ [10]. In these materials many experiments to exchange H^+ ion by Li^+ have failed. It was explained by that strong hydrogen bonding linking triphosphate groups might be fundamental to sustain the structure.

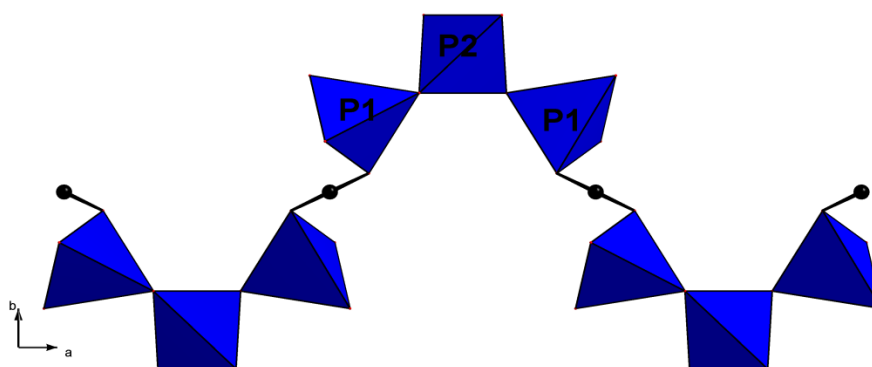


Figure 4. Projection of $[\text{HP}_3\text{O}_{10}^{4-}]^n$ along c direction.

The P–O distances range from $1.492(5)$ to $1.606(6)$ \AA for P1O_4 and vary from $1.503(5)$ to $1.584(6)$ \AA for P2O_4 tetrahedra. The distance P–P is (2.883\AA) and the angle P–P–P is $111.69(6)$. The geometry of P_3O_{10} group is very similar to that of its isotype [7]. It was shown in the literature that tetrahedra distortion is very common in triphosphates [7, 9, 10].

Thallium cations partially occupy their sites and Tl-O distances vary from 2,864 (9) to 3,418 (6) Å for Tl1 and from 2.85 (2) to 3.63 (4) Å for Tl2 (Table 5). These thallium distances are in agreement with values met in the literature [40].

Table 5. Interatomic distances (Å) in the structure for TlFeHP₃O₁₀.

P1 tetrahedron		P2 tetrahedron	
P2—O4 ^x	1.502 (5)	P1—O3	1.492 (5)
P2—O4	1.502 (5)	P1—O1	1.512 (6)
P2—O2 ^x	1.584 (6)	P1—O6	1.515 (5)
P2—O2	1.584 (6)	P1—O2 ⁱⁱ	1.606 (6)
Fe1 octahedron			
Fe1—O3 ⁱ	1.968 (5)	Fe1—O6 ⁱⁱⁱ	1.987 (5)
Fe1—O3 ⁱⁱ	1.968 (5)	Fe1—O4 ⁱⁱ	1.994 (5)
Fe1—O6	1.987 (5)	Fe1—O4 ⁱ	1.994 (5)
Tl1 polyhedron		Tl2 polyhedron	
Tl1—O1 ^{ix}	2.864 (9)	Tl2—O1 ^{ix}	2.85 (2)
Tl1—O3 ^{xiii}	3.089 (7)	Tl2—O3 ^{xi}	3.02 (2)
Tl1—O3 ^{xi}	3.089 (7)	Tl2—O6 ^{xi}	3.08 (4)
Tl1—O4 ^{xiii}	3.15 (1)	Tl2—O4 ^{xiii}	3.13 (2)
Tl1—O4 ^{xi}	3.15 (1)	Tl2—O3 ^{xiii}	3.23 (2)
Tl1—O6 ^{xi}	3.348 (5)	Tl2—O6 ^{xiv}	3.29 (2)
Tl1—O6 ^{xiii}	3.348 (5)	Tl2—O4 ^{xi}	3.29 (1)
Tl1—O6 ^{xiv}	3.418 (6)	Tl2—O6 ^{iv}	3.60 (3)
Tl1—O6 ^{iv}	3.418 (6)	Tl2—O6 ^{xiii}	3.63 (4)
<p>Symmetry codes: (i) $x, -y+1, z+1/2$; (ii) $-x+1/2, y+1/2, -z+1/2$; (iii) $-x+1/2, -y+3/2, -z+1$; (iv) $-x+1/2, -y+1/2, -z+1$; (v) $x, y+1, z$; (vi) $x+1/2, -y+1/2, z+1/2$; (vii) $-x, y+1, -z+1/2$; (viii) $x+1/2, y+1/2, z$; (ix) $-x, y, -z+1/2$; (x) $-x+1, y, -z+1/2$; (xi) $-x+1/2, y-1/2, -z+1/2$; (xii) $-x+1/2, -y+1/2, -z$; (xiii) $x-1/2, y-1/2, z$; (xiv) $x-1/2, -y+1/2, z-1/2$.</p>			

3.2. Pathways transport simulation proposed from bond valence analysis

3.2.1 Alkali pathways transport simulation by BVSP

The bond valence sum path (BVSP) showed that small tunnels, extending along [011], are not favourable for thallium cations mobility. Cations meet bottlenecks of the valence unit maxima $Vu_{max} = 1.55$ for an only 2.3 Å covered distance (Fig. 5).

Tl⁺ migration seems to be easier only along *c*-axis (Fig. 6b). However, Vu_{max} for thallium migration along this direction reaches 1.367u.v for a 2.81Å distance. In fact, the bottleneck widths of the tunnels vary from 4.825 Å to 5,709 Å 4.943 Å which are smaller than the geometrical size sum of 6.08 Å corresponding to $2 \times (r_{Tl^+} + r_{O^{2-}}) = 2 \times (1.64 + 1.40) \text{Å}$ (Fig. 6a).

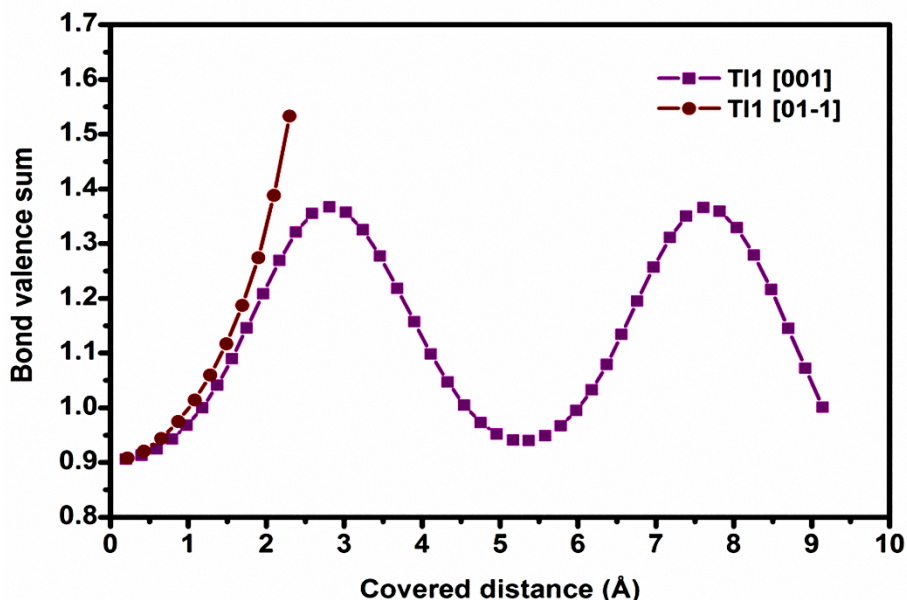


Figure 5. Bond valence sum for thallium ions vs. the covered distance.

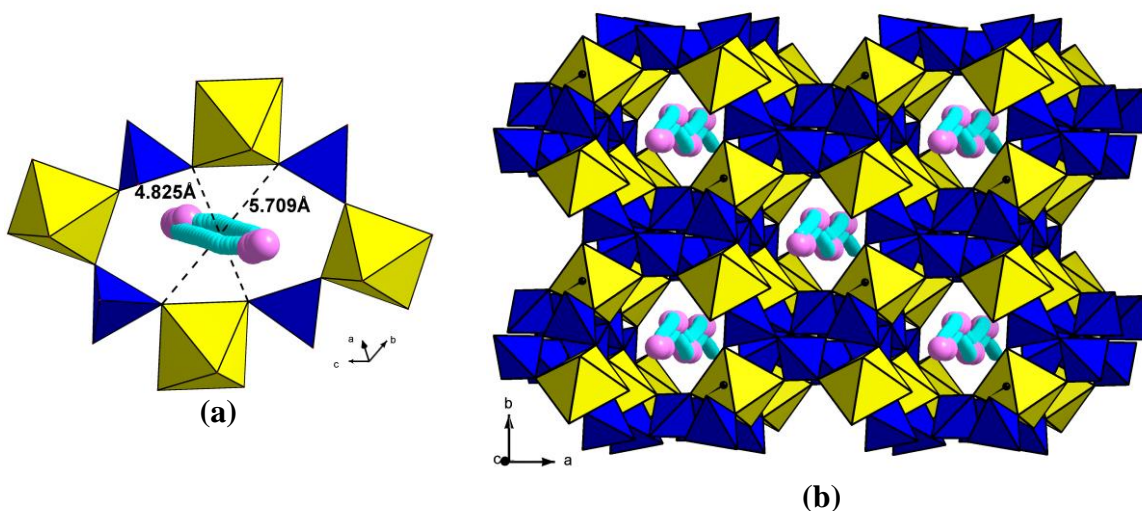


Figure 6. (a) Geometrical and size of tunnels parallel to *c*-axis.(b) The minimum BVS mismatch path along the [001] direction for Tl^+ , determined using the JUMPITER software.

3.2.2. Alkali pathways transport simulation by BVSE

The bond valence site energy (BVSE) showed that thallium migration is one-dimensional along *c* direction. Although tunnels size is slightly lower than the geometrical size sum of oxygen and thallium diameters low migration energy $E_{mig} = 0.664$ eV was observed (Fig. 7). The same phenomenon was noted in $TlFe_{0.22}Al_{0.78}As_2O_7$ [41,42]. This material showed a one-dimensional migration path of thallium atoms with experimental and theoretical activation energies equal to 0.656 and 0.6 eV respectively.

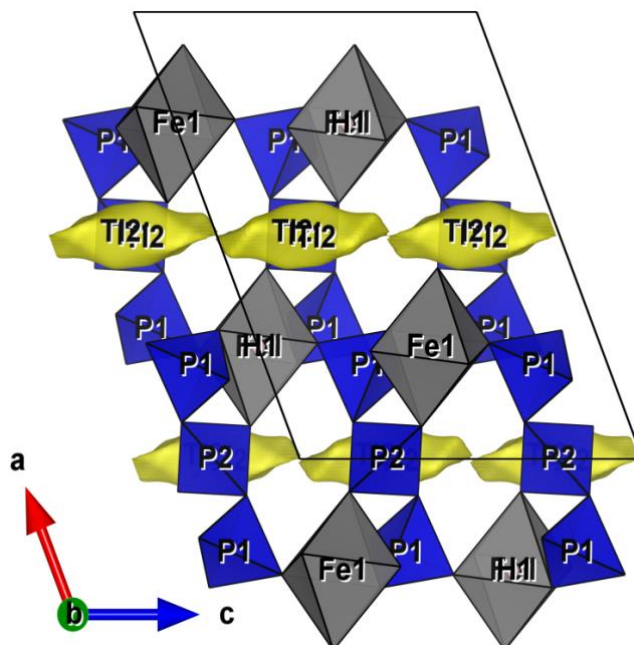


Figure 7. 1D migration pathways of thallium cation along c axis at $E_{\text{mig}} = 0.664$ eV.

The BVSE is usually used to model alkali metal cations conduction pathways in the crystal bulk [43-48]. However, It was successfully employed to determine proton migration model in $\text{Fe}^{2+}\text{Fe}^{3+}_{3.2}(\text{Mn}^{2+}, \text{Zn})_{0.8}(\text{PO}_4)_3(\text{OH})_{4.2}(\text{H}_2\text{O})_{0.8}$ [49].

The bond valence site energy showed that proton migration is three-dimensional. At a migration energy equal to 0.682 eV, proton migration channels along [110] and [-110] directions were observed (Fig. 8). Despite thallium cations, protons are located in small cavities. However, their small size allowed them to migrate at almost the same energy for one dimensional direction.

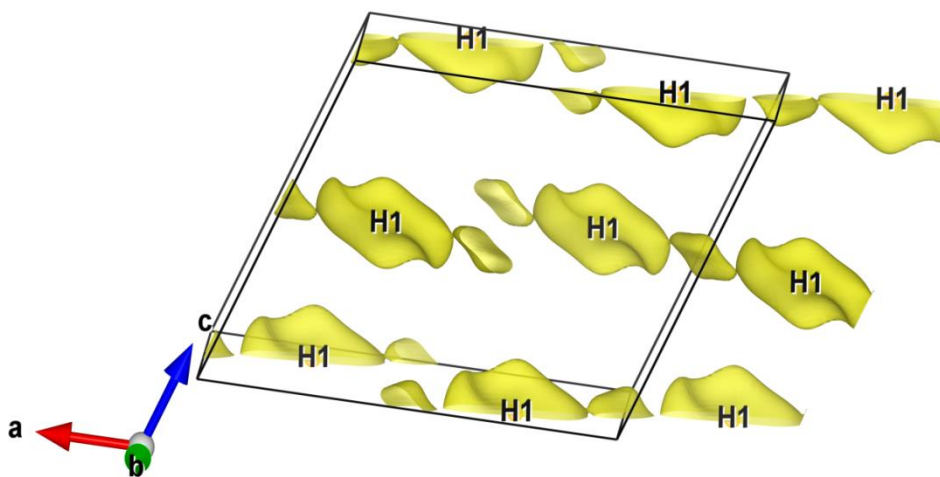


Figure 8. 1D migration pathways of H^+ cation along [110] and [-110] directions at $E_{\text{mig}} = 0.682$ eV.

Then each channel formed previously along the same direction is connected in (001) Plan at a migration energy 1.203 eV (Fig. 9). The proton percolates in order to connect migration sheets at energy equal to 1.293 eV. The BVSE shows that proton diffusion was not only allowed by conventional proton crystallographic sites and structurally-equivalent sites in the neighbouring unit cells but also insured by interstitials (Fig. 10). Proton percolation over interstitials was also observed in the $\text{Cs}_3\text{H}(\text{SeO}_4)_2$, $\text{Rb}_3\text{H}(\text{SeO}_4)_2$, KH_2PO_4 and the one and zero dimensional CsH_2PO_4 and $\text{Me}_3\text{H}(\text{AO}_4)_2$ materials respectively [50-51].

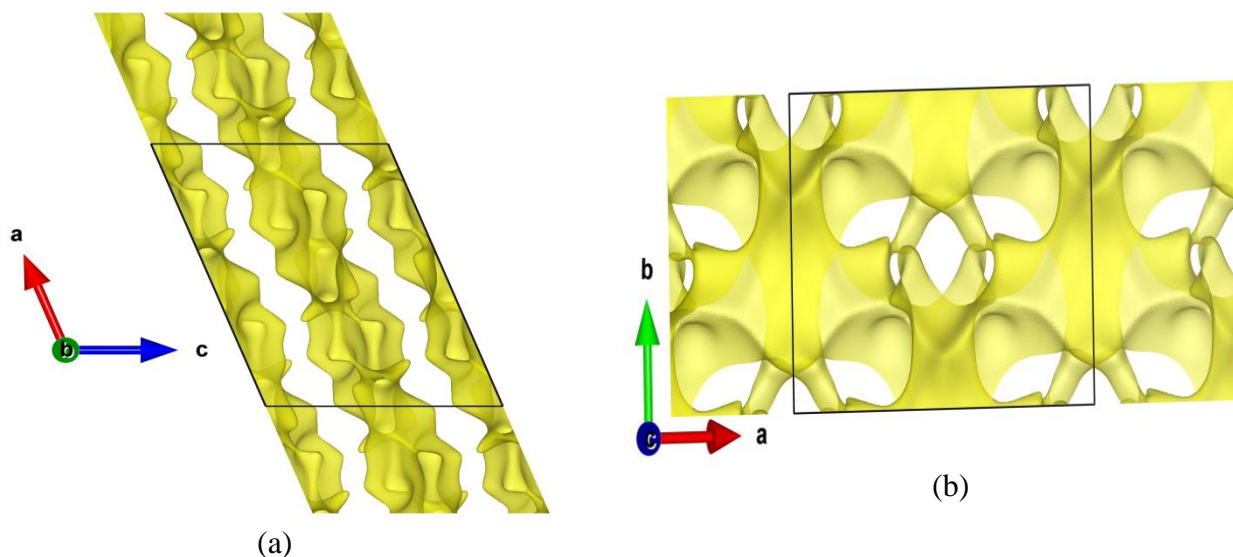


Figure 9. Projection of 2 D conduction pathways migrations of H^+ at $E_{\text{mig}}= 1.203$ eV (a) Along b direction (b) Along c direction.

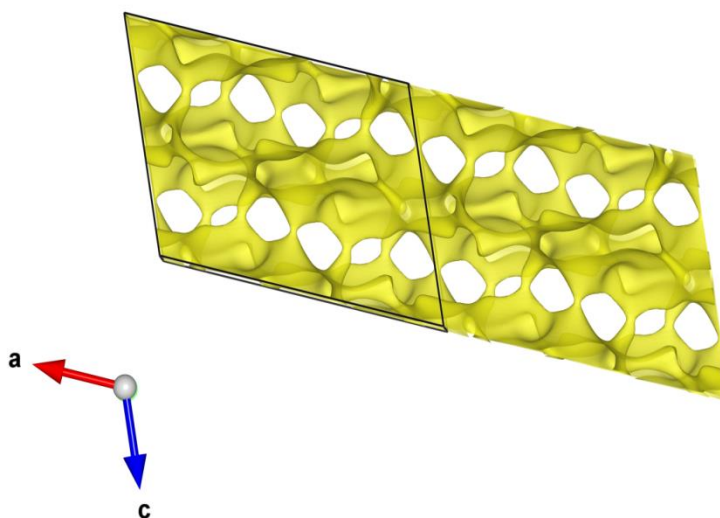


Figure 10. Projection of 3 D conduction pathways migrations of H^+ along b axis at $E_{\text{mig}}= 1.293$ eV.

It can be deduced from this study that protons are the most responsible moving species for ionic conduction of this material. Nevertheless, thallium contribution ameliorates the ionic conductivity. As a result, TlFeHP₃O₁₀ can be a good candidate for battery electrode material.

3.3. IR spectroscopy

Since the most significant absorption bands of the P₃O₁₀ group are located between 1500 and 400 cm⁻¹, we are interested in this domain (Fig. 11). Frequencies assignments of the P₃O₁₀⁵⁻ anion are based on the characteristic vibrations of the P–O–P bridge, PO₂ and PO₃ groups. The band observed at 1352 cm⁻¹ was attributed to (P=O) vibration which was also observed in the NiNa₃P₃O₁₀.12H₂O infrared spectra [53] (Table 6). The bands generated by the symmetric and antisymmetric-stretching frequencies of PO₂ and PO₃ in P₃O₁₀⁵⁻ are detected at 1143 and 1054 cm⁻¹ respectively. Since P–O bonds in PO₂ and PO₃ groups are weaker than bonds in the P–O–P bridge, then the vibrational frequencies of PO₂ and PO₃ are likely higher than those for P–O–P. So bands found in the region 987–624 cm⁻¹ are ascribed to the antisymmetric and symmetric P-O-P stretching modes.

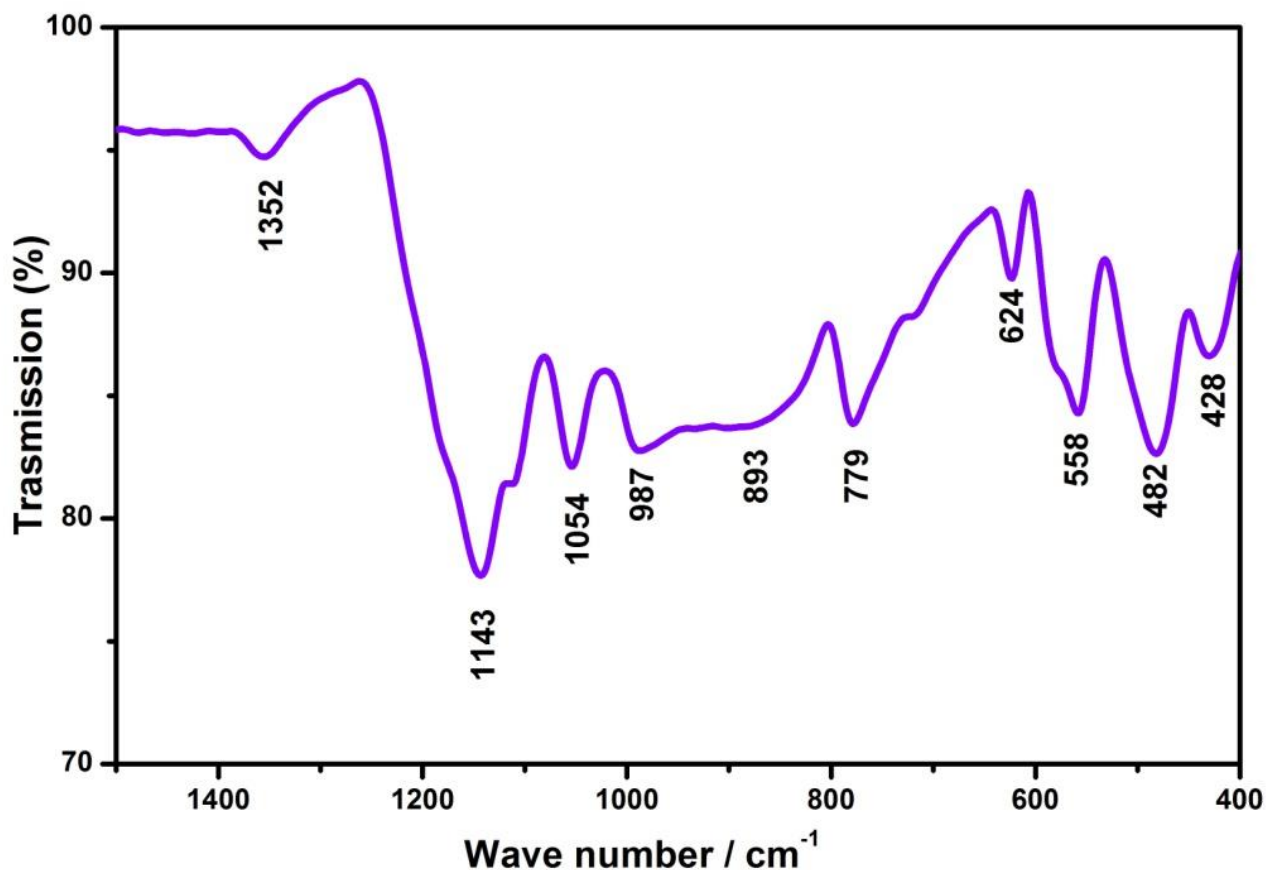


Figure 11. Infrared spectrum of TlFeHP₃O₁₀.

Table 6. Frequencies of the main IR vibrations (cm^{-1}) of P_3O_{10} or HP_3O_{10} entities encountered in the bibliography data

Attribution ref.	$\text{NiNa}_3\text{P}_3\text{O}_{10} \cdot 12\text{H}_2\text{O}$ [53]	$\text{KYHP}_3\text{O}_{10}$ [35]	$\text{K}_{0.24}(\text{NH}_4)_0.76\text{YHP}_3\text{O}_{10}$ [54]	$\text{NH}_4\text{YHP}_3\text{O}_{10}$ [54]	$\text{RbPrHP}_3\text{O}_{10}$ [14]	$\text{KDyHP}_3\text{O}_{10}$ [36]	$\text{KMnHP}_3\text{O}_{10}$ [10]	$\text{TlFeHP}_3\text{O}_{10}$ (This work)
ν_{OH} (P-OH)	-	2922 2371	2838 2370	2838 2370	-	2925 2370	2917 2361	-
ν (P=O)	1355	1264	1258	1256	1255	1262 1200	1248 1182	1352
$\nu_{\text{as}}(\text{PO}_2) + \nu_{\text{s}}(\text{PO}_2)$ + $\nu_{\text{as}}(\text{PO}_3) + \nu_{\text{s}}(\text{PO}_3)$	1277 1188 1059 1002	1202 1129 1101 1066 1036 1013	1186 1125 1106 1064 1038 1015	1184 1125 1101 1065 1039 1014	1122 1095 1051 1035 1010	1128 1100 1065 1036 1012	1116 1088 1037 1029 1006	1143 1054
$\nu_{\text{as}}(\text{POP})$	908	976 937	973 937	973 939	970 930	978 936	936 925	987
$\nu_{\text{s}}(\text{POP})$	799 700 650	833 783 701	835 783 701	833 783 701	839 773 696 625	835 782 700	833 764 689	893 779 624
Deformation vibrations + M-O vibrations (M = Mn, Ni, Fe, Y, Pr, Dy)	600 544	612 586 560 536 514 485 434	611 584 561 536 512 485 434	611 585 563 536 513 486 435	605 578 551 530 513 480 428	611 586 560 532 514 485 433	599 568 542 528 508 474 423	558 482 430

4. CONCLUSION

New phosphate $\text{TlFeHP}_3\text{O}_{10}$ was synthesized by hydrothermal method. The structure has been solved and confirmed by X-ray diffraction and BVS and CHARDI methods respectively. The compound is formed by triphosphate groups HP_3O_{10} and FeO_6 octahedra connected by corners. The structure of this material has an open framework having tunnels along c axis where thallium cations reside. Conduction migration pathways of thallium and proton were investigated using BVSP and BVSE models. Migration energies for one dimensional thallium migration and three dimensional proton migrations were 0.664 eV and 1.293 eV respectively. These values present a quite fast ionic conductivity.

SUPPLEMENTARY INFORMATION

Crystallographic data for $\text{TlFeHP}_3\text{O}_{10}$ has been deposited with the Cambridge Crystallographic Data Centre as supplemental publication numbers (CCDC)2008094. Copies of the data can be obtained free of charge via <http://www.ccdc.cam.ac.uk>.

ACKNOWLEDGEMENT

The authors extend their appreciation to the Deanship of Scientific Research at King Khalid University, Abha, Saudi Arabia for funding this work through General Research Project under grant number R.G.P.1/230/41 (Inorganic materials and applications Group).

References

1. R. Khaoulaf, K. Brouzi, A. Ennaciri, M. Harcharras and F. Elhafiane, *J. Mater. Environ. Sci.*, 8 (2017) 2893.
2. J. Gao, X. Liu, L. Song, X. Sha, P. Zhao and P. Guo, *Solid state sci.*, 55 (2016) 163.
3. L.V. Shvanskaya, O.V. Yakubovich and V.I. Belik, *Crystallogr. Rep.*, 61 (2016) 795.
4. B. Klinkert and M. Jansen, *Z. Elektrochem. Angew. Phys. Chem.*, 567 (1988) 86.
5. M.A. Vaivada, Z.A. Konstant and V.V. Krasnikov, *Neorg. Mater.*, 21 (1985) 1559.
6. M.T. Averbuch-Pouchot and J. C. Guitel, *Acta Crystallogr., Sect. B: Struct. Sci.*, 33 (1977) 1615.
7. V.V. Krasnikov, Z.A. Konstant and V.S. Fundamensii, *Neorg. Mater.*, 19 (1983) 1378.
8. M.T. Averbuch-Pouchot, A. Durif and J.C. Guitel, *Acta. Crystallogr., Sect. B: Struct. Sci.*, 33 (1977) 1438.
9. A.J. Wright, C. Ruiz-Valero, J.P. Attfield, *J. Solid State Chem.*, 145 (1999) 483.
10. A.J. Wright, J.P. Attfield, *Inorg. Chem.*, 37 (1998) 3861.
11. N. Zouari, T. Mhiri, A. Daoud, P. Gravereau, E. Lebraud, *Int. J. Inorg. Mater.*, 2 (2000) 387.
12. M.T. Averbuch-Pouchot, M. BagieuBeucher, *Z. Elektrochem. Angew. Phys. Chem.*, 552 (1987) 180.
13. N. Anisimova, M. Bork, R. Hoppe, M. Meisel, *Z. Elektrochem. Angew. Phys. Chem.*, 621 (1995) 1074.
14. K.H. Naifer, M. Ferid and M.T. Ayadi, *Mater. Res. Bull.*, 40(2005) 314.
15. J. Mechergui, W. Belam, *Mater. Res. Bull.*, 43 (2008) 3367.
16. A.J.M. Duisenberg, *J. Appl. Crystallogr.*, 25 (1992) 92.
17. J. Maciček, A. Yordanov, *J. Appl. Crystallogr.*, 25 (1992) 73
18. G. M. Sheldrick, *Acta Crystallogr., Sect. A: Found. Crystallogr.*, 64 (2008) 122.
19. L.J. Farrugia, *J. Appl. Crystallogr.*, 32 (1999) 837.
20. A.C.T. North and D.C. Phillips, F.S. Mathews, *Acta Crystallogr., Sect. A: Found. Crystallogr.*, 24 (1968) 359.
21. A. Linden, K.W. Nugent, A. Petridis, B.D. James, *Inorg. Chim. Acta*, 285 (1999) 128
22. M. Nespolo, G. Ferraris, G. Ivaldi and R. Hoppe, (2001). *Acta Crystallogr., Sect. B: Struct. Sci.*, 57 (2001) 664.
23. M. Nespolo, B. Guillot, *J. Appl. Crystallogr.*, 49 (2016) 321.
24. O.S.A. ALQarni, R. Marzouki, Y. Ben Smida, M.M. Alghamdi, M. Avdeev, R. BelhadjTahar and M.F. Zid, *Processes*, 8 (3) (2020) 305.
25. I.D. Brown, *The Chemical Bond in Inorganic Chemistry – The Bond Valence Model*. IUCr, Monographs on Crystallography, Vol. 12, Oxford University
26. M. Nespolo, (2015) CHARDT2015. A program to compute the Effective Coordination Number (ECoN) and the Charge Distribution in non-molecular crystal structures (<http://crm2.univlorraine.fr/lab/fr/software/chardi2015/>)
27. S. Adams, O. Moretzki and E. Canadell, *Solid State Ionics*, 168 (2004) 281.
28. S. Adams, *Acta Crystallogr., Sect. B: Struct. Sci.*, 57 (2001) 287.
29. I.D. Brown, *Chem. Rev.*, 109 (2009) 6858.
30. S. Adams, *Solid State Ionics*, 177 (2006) 1625.
31. S. Adams and R.P. Rao, *Phys. Status Solidi A*, 208 (2011) 1746.
32. D. Mazza, *J. Solid State Chem.*, 156 (2001) 154.
33. S. Adams and R.P. Rao, *Atom Indonesia*, 36 (2010) 95.

34. K. Momma and F. Izumi, *J. Appl. Crystallogr.*, 44 (2011) 1276.
35. N. Zouari, H. Khemakhem, T. Mhiri, A. Daoud, *J. Phys. Chem.*, 60 (1999) 1779.
36. N. Zouari, M. Mnif, H. Khemakhem, T. Mhiri, A. Daoud, *Solid State Ionics*, 110 (1998) 269.
37. F.C. Coomer, N.J. Checker, A.J. Wright, *Adv. Inorg. Chem.*, 49 (2010) 943.
38. E.V. Murashova, N.N. Chudinova, *Crystallogr. Rep.*, 40 (1995) 441.
39. M. Jinxiao, H. Borrmann, Y.X. Huang, J.T. Zhao, *Z. Kristallogr. - New Cryst. Struct.*, 218 (2003) 168.
40. I.D. Brown and R. Faggiani, *Acta. Crystallogr., Sect. B: Struct. Sci.*, 36 (1980) 1806.
41. N. Ouerfelli, A. Guesmi, D. Mazza, A. Madani, M.F. Zid and A. Driss, *J. Solid State Chem.*, 180 (2007) 1229
42. M. Sale and M. Avdeev, *J. Appl. Crystallogr.*, 45 (2012) 1056
43. M.A. Ben Moussa, R. Marzouki, A. Brahmia, S. Georges, S. Obbade and M.F. Zid, *Int. J. Electrochem. Sci.*, 14 (2019) 1500.
44. E. Rezugui, A. Souilem, C. Issaoui, N. Ouerfelli and M.F. Zid, *Int. J. Electrochem. Sci.*, 15 (2020) 5894.
45. Y. Ben Smida, R. Marzouki, S. Georges, R. Kutteh, M. Avdeev, A. Guesmi, M.F. Zid, *J. Solid State Chem.*, 239 (2016) 8.
46. R. Marzouki, Y. Ben Smida, M. Sonni, M. Avdeev, M.F. Zid, *J. Solid State Chem.*, 285 (2020) 121058.
47. R. Marzouki and M. F. Zid, *Int. J. Electrochem. Sci.*, 15 (2020) 3792.
48. R. Marzouki, *Mater. Res. Express*, 7 (2020) 016313.
49. M. Winklera, P. Lunkenheimera, A. Loidla, S.H. Parkb, B. Röskab and M. Hoelzelc, *Solid State Ionics*, 347 (2020) 240.
50. A.I. Baranov, B.V. Merinov, A.B. Tregubchenko, L.A. Shuvalov and N.M. Shchagina, *Ferroelectr. Lett.*, 81(1988) 191
51. A.I. Baranov, V.P. Khiznichenko and L.A. Shuvalov, *Ferroelectr. Lett.*, 100 (1989) 135.
52. A.I. Baranov, V.P. Khiznichenko, V.A. Sandler, and L.A. Shuvalov, *Ferroelectr. Lett.*, 81 (1988) 183.
53. M. Tridane, I. Fahim, S. Benmokhtar and S. Belaaouad, *The Japan Science and Technology Information Aggregator, Electronic*, 30 (2015) 7.
54. A. Hammady, Préparation, Etude Structurale et Physico-chimique de Phosphates Condense's d'yttrium et des Cations Monovalents: H, Li, Na, K, NH et Divalents: Ca., PhD Thesis, Tunisia, University of Tunis II (FST), 1996.